0026-895X/06/6906-1801–1809$20.00
MOLECULAR PHARMACOLOGY
Copyright © 2006 The American Society for Pharmacology and Experimental Therapeutics
Mol Pharmacol 69:1801–1809, 2006

Vol. 69, No. 6
21899/3114611
Printed in U.S.A.

Development of a Novel Nitro-Derivative of Noscapine for the Potential Treatment of Drug-Resistant Ovarian Cancer and T-Cell Lymphoma

Ritu Aneja, Surya N. Vangapandu, Manu Lopus, Ramesh Chandra, Dulal Panda, and Harish C. Joshi

Laboratory for Drug Discovery and Research, Department of Cell Biology, Emory University School of Medicine, Atlanta, Georgia (R.A., S.N.V., H.C.J.); B. R. Ambedkar Center for Biomedical Research (R.C.), University of Delhi, India and School of Biosciences and Bioengineering, Indian Institute of Technology Bombay (M.L., D.P.), Mumbai, India

Received December 20, 2005; accepted March 1, 2006

ABSTRACT

We have shown previously that an antitussive plant alkaloid, noscapine, binds tubulin, displays anticancer activity, and has a safe pharmacological profile in humans. Structure-function analyses pointed to a proton at position-9 of the isoquinoline ring that can be modified without compromising tubulin binding activity. Thus, many noscapine analogs with different functional moieties at position-9 were synthesized. Those analogs that kill human cancer cells resistant to other antimicrotubule agents, *vincas* and *taxanes*, were screened. Here, we present one such analog, 9-nitro-noscapine (9-nitro-nos), which binds tubulin and induces apoptosis selectively in tumor cells (ovarian and T-cell lymphoma) resistant to paclitaxel, vinblastine, and teniposide. 9-Nitro-nos treatment at doses as high as 100 μM did not affect the cell cycle profile of normal human fibroblasts. This selectivity of 9-nitro-nos for cancer cells represents a unique edge over the other available antimitotics. 9-Nitro-nos perturbs the progression of cell cycle by mitotic arrest, followed by apoptotic cell death associated with increased caspase-3 activation and appearance of terminal deoxynucleotidyl transferase dUTP nick-end labeling-positive cells. Thus, we conclude that 9-nitro-nos has great potential to be a novel therapeutic agent for ovarian and T-cell lymphoma cancers, even those that have become drug-resistant to currently available chemotherapeutic drugs.

Microtubules are major cytoskeletal structures responsible for maintaining genetic stability during cell division (Sammak and Borisy, 1987). The dynamics of these polymers are absolutely crucial for this function that can be described as their growth rate at the plus ends, catastrophic shortening, frequency of transition between the two phases, pause between the two phases, their release from the microtubule organizing center, and treadmilling (Kirschner and Mitchison, 1986; Zhou and Giannakakou, 2005). Microtubule lattice also serves as tracks for the axonal transport of organelles driven by anteriograde and retrograde molecular motors to generate and maintain axonal integrity (Joshi, 1998). Interference with microtubule dynamics often leads to programmed cell death, and thus, microtubule-binding drugs are currently used to treat various malignancies in the clinic (Jordan and Wilson, 2004). Although useful, currently used microtubule drugs such as *vincas* and *taxanes* are limited because of the emergence of drug resistance. There have been multiple mechanisms for antimicrotubule drug resistance, including overexpression of drug-efflux pumps, misexpression of tubulin isotypes, and perhaps mutational lesions in tubulin itself (Ranganathan et al., 1996; Giannakakou et al., 1997; Monzo et al., 1999; Dumontet et al., 2005).

The pharmacological profile of microtubule-binding agents, however, has not been ideal. Most of them need to be infused over long periods of time in the clinic because they are not water-soluble and can cause hypersensitive reactions because of the vehicle solution (Rowinsky, 1997). Furthermore, normally dividing cells within the healthy tissues such as intestinal crypts, hair follicles, and bone marrow are also vulnerable to these agents, leading to toxicities (Rowinsky,

This work was supported by funding from the National Institutes of Health (to H.C.J.) and partly from the Department of Biotechnology, India (to D.P.).
Article, publication date, and citation information can be found at http://molpharm.aspetjournals.org.
doi:10.1124/mol.105.021899.

ABBREVIATIONS: 9-nitro-nos, 9-nitro-noscapine; PIPES, piperazine-*N*,*N*′-bis(2-ethanesulfonic acid); PBS, phosphate-buffered saline; BSA, bovine serum albumin; HPLC, high-performance liquid chromatography; MTS, 3-(4,5-dimethylthiazol-2-yl)-2,5-diphenyl tetrazolium bromide; TUNEL, terminal deoxynucleotidyl transferase dUTP nick-end labeling; TdT, terminal deoxynucleotidyl transferase; BrdUTP, bromo-deoxyuridine triphosphate; PI, phosphatidylinositol; TFAA, trifluoroacetic anhydride; Pgp, P-glycoprotein.

1997). In addition, nerve cells dependent on molecular traffic over long distances undergo degenerative changes, causing peripheral neuropathies (Pace et al., 1996; Crown and O'Leary, 2000; Theiss and Meller, 2000; Topp et al., 2000).

We have discovered recently that noscapine, a safe antitussive agent for more than 40 years, binds tubulin, arrests dividing cells in mitosis, and induces apoptosis (Ye et al., 1998). It is well-tolerated in humans and has been shown to be nontoxic in healthy volunteers, including pregnant mothers (Dahlstrom et al., 1982; Karlsson et al., 1990; Jensen et al., 1992). Unlike the other microtubule-targeting drugs, noscapine does not significantly change the microtubule polymer mass, even at high concentrations. Instead, it suppresses microtubule dynamics by increasing the time that microtubules spend in an attenuated (pause) state when neither microtubule growth nor shortening is detectable (Landen et al., 2002). Thus, noscapine-induced suppression of microtubule dynamics, even though subtle, is sufficient to interfere with the proper attachment of chromosomes to kinetochore microtubules and to suppress the tension across paired kinetochores (Zhou et al., 2002b). This represents an improvement over the *taxanes* (the microtubule-bundling agents or overpolymerizers) and *vincas* (the depolymerizers) that cause toxicities in mitotic and postmitotic neurons at elevated doses. Noscapine thus effectively inhibits the progression of various cancer types both in cultured cells and in animal models with no obvious side effects (Ye et al., 1998; Landen et al., 2002, 2004; Zhou et al., 2002a, 2003). It is surprising that the apoptosis is much more pronounced in cancer cells than in normal healthy cells (Landen et al., 2002). Furthermore, we have done extensive structure-activity relationship studies, producing a battery of analogs of which two analogs have shown potent activity against cancer cells without detectable toxicities (Checchi et al., 2003; Zhou et al., 2003, 2004, 2005). The parent compound noscapine itself is also active against cancer cells, including drug-resistant variants, albeit at high concentrations.

In this study, we present the synthesis, characterization, and evaluation of the antitumor potential of a novel nitro analog of noscapine, 9-nitro-nos, which binds tubulin and effectively inhibits cell proliferation of 1A9 (ovarian cancer cells) and its paclitaxel-resistant variant (1A9/PTX22) and human lymphoblastoid cells CEM, and its vinblastine-(CEM/VLB100) and teniposide (CEM/VM-1-5)-resistant variants. 9-Nitro-nos treatment selectively halts cell cycle progression at the G_2/M phase in cancer cells without affecting the cell cycle of normal human fibroblast cells. This mitotic catastrophe in cancer cells is then followed by the induction of apoptosis. The apoptotic mechanism is associated with the activation of the key executioner cysteine protease, caspase-3. Most importantly, 9-nitro-nos is more potent against cancer cells that have become resistant to currently used drugs, like vinblastine, teniposide, and paclitaxel, compared with their respective sensitive-parent lines.

Materials and Methods

Chemistry

^{1}H NMR and ^{13}C NMR spectra were measured by 400 NMR spectrometer in a $CDCl_3$ solution and were analyzed by INOVA (Varian, Inc., Palo Alto, CA). Proton NMR spectra were recorded at 400 MHz and were referenced with residual chloroform (7.27 ppm). Carbon NMR spectra were recorded at 100 MHz and were referenced with 77.27 ppm of resonance of residual chloroform. Abbreviations for signal coupling are as follows: s, singlet; d, doublet; t, triplet; q, quartet; m, multiplet. Infrared spectra were recorded on sodium chloride discs on Mattson Genesis II FT-IR 9 (Thermo Electron Corporation, Waltham, MA). High-resolution mass spectra were collected on Thermo Finnigan LTQ-FT Hybrid mass spectrophotometer using 3-nitrobenzyl alcohol or with the addition of LiI as a matrix. Melting points were determined using a Thomas-Hoover melting point apparatus and were uncorrected. All reactions were conducted with oven-dried (125°C) reaction vessels in dry argon. All common reagents and solvents were obtained from Aldrich Chemical Co. (Milwaukee, WI) and were dried using 4 Å molecular sieves. The reactions were monitored by thin-layer chromatography using silica gel 60 F254 (Merck, Whitehouse Station, NJ) on precoated aluminum sheets. Flash chromatography was carried out on standard-grade silica gel (230–400 mesh).

Synthesis of 9-Nitro-nos

To a solution of noscapine (4.134 g, 10 mmol) in acetonitrile (50 ml), silver nitrate (1.70 g, 10 mmol) and trifluoroacetic anhydride (5 ml, 35 mmol) were added. After 1 h of reaction time, the reaction progress was monitored using thin-layer chromatography (10% methanol in chloroform), and the reaction mixture was poured into 50 ml of water and extracted with chloroform (3 × 50 ml). The organic layer was washed with brine, dried over anhydrous magnesium sulfate, and the solvent was evaporated in vacuo. The desired product, (*S*)-6,7-dimethoxy-3-((*R*)-4-methoxy-6-methyl-9-nitro-5,6,7,8-tetrahydro-[1,3]dioxolo[4,5-*g*]isoquinolin-5-yl)isobenzofuran-1(3*H*)-one (9-nitro-nos) was obtained as yellow crystalline powder by flash chromatography (silica gel, 230–400 mesh) with 10% methanol in chloroform as an eluent; melting point, 178.2–178.4°C; IR: 1529, 1362 cm^{-1}; ^{1}H NMR ($CDCl_3$, 400 MHz): δ 7.27 (d, 1H, J = 8.0 Hz), 7.08 (d, 1H, J = 8.0 Hz), 6.02 (s, 2H), 5.91 (d, 1H, J = 4.1 Hz), 4.42 (d, 1H, J = 4.1 Hz), 4.09 (s, 3H), 3.89 (s, 3H), 3.83 (s, 3H), 2.74–2.64 (m, 2H), 2.61–2.56 (m, 2H), 2.52 (s, 3H); ^{13}C NMR ($CDCl_3$, 100 MHz): δ 169.7, 157.2, 151.6, 147.5, 142.3, 140.5, 135.0, 134.2, 123.2, 120.8, 119.9, 119.4, 114.1, 100.8, 87.6, 63.7, 56.8, 56.4, 56.1, 51.4, 39.2, 27.0; HRMS (ESI): m/z calculated for $C_{22}H_{23}N_2O_9$ (M + 1), 459.4821; found, 459.4755 (M + 1).

HPLC Purity and Peak Attributions

The HPLC purity was determined after two different methods using varied solvent systems: Method 1: Ultimate Plus, LC Packings, Dionex, C_{18} column (pep Map 100, 3 μm; particle size, 100 Å; internal diameter, 1000 μm; length, 15 cm) with solvent systems A (0.1% formic acid in water) and B (acetonitrile); gradient, 25-min run at a flow of 40 μl/min. Retention time for 9-nitro-nos is 19.30 min. HPLC purity was 96%. Method 2: Ultimate Plus, LC Packings, Dionex, C_{18} column (pep Map 100, 3 μm; particle size, 100 Å; internal diameter, 1000 μm; length, 15 cm) with solvent systems A (0.1% formic acid in water) and B (methanol); gradient, 25-min run at a flow of 40 μl/min. Retention time for 9-nitro-nos is 19.86 min. HPLC purity was 97%.

Cell Lines and Chemicals

Cell culture reagents were obtained from Mediatech (Herndon, VA). CEM, a human lymphoblastoid line, and its drug-resistant variants CEM/VLB100 and CEM/VM-1-5 were provided by Dr. William T. Beck (Cancer Center, University of Illinois at Chicago, Chicago, IL). CEM-VLB100, a multidrug-resistant line selected against vinblastine, is derived from the human lymphoblastoid line CEM and expresses high levels of 170-kDa P-glycoprotein (Beck and Cirtain, 1982). CEM/VM-1-5, resistant to the epipodophyllotoxin teniposide (VM-26), expresses a much higher amount of MRP protein than CEM cells (Morgan et al., 2000). The 1A9 cell line is a clone of the human ovarian carcinoma cell line, A2780. The paclitaxel-resistant cell line 1A9/PTX22 was isolated as an individual clone in a

single-step selection by exposing 1A9 cells to 5 ng/ml paclitaxel in the presence of 5 μg/ml verapamil, a P-glycoprotein antagonist (Giannakakou et al., 1997). All cells were grown in RPMI 1640 medium (Mediatech, Herndon, VA) supplemented with 10% fetal bovine serum (Invitrogen, Carlsbad, CA) and 1% penicillin/streptomycin (Mediatech). Paclitaxel-resistant 1A9/PTX22 cell line was maintained in 15 ng/ml paclitaxel and 5 μg/ml verapamil continuously but was cultured in drug-free medium for 7 days before the experiment. Human primary fibroblasts were cultured by digestion and trituration of prepuces of circumcised male babies. They were washed in sterile saline five times and cut into small pieces before incubation with trypsin in Dulbecco's modified Eagle's medium 1× for 30 min. Tissue clumps were removed, and fibroblasts were plated onto culture dishes that were maintained at 37°C in 5% CO_2 atmosphere in Dulbecco's modified Eagle's medium with 4.5 g/l glucose and L-glutamine (Mediatech) supplemented with 10% fetal bovine serum and 1% penicillin/streptomycin. Mammalian brain microtubule proteins were isolated by two cycles of polymerization and depolymerization, and tubulin was separated from the microtubule binding proteins by phosphocellulose chromatography as described previously (Panda et al., 2000; Joshi and Zhou, 2001). The tubulin solution was stored at −80°C until use.

Tubulin Binding Assay

Fluorescence titration for determining the tubulin binding parameters was performed as described previously (Gupta and Panda, 2002). In brief, 9-nitro-nos (0–100 μM) was incubated with 2 μM tubulin in 25 mM PIPES, pH 6.8, 3 mM $MgSO_4$, and 1 mM EGTA for 45 min at 37°C. The relative intrinsic fluorescence intensity of tubulin was then monitored in a JASCO FP-6500 spectrofluorometer (JASCO, Tokyo, Japan) using a cuvette of 0.3 cm path length, and the excitation wavelength was 295 nm. The fluorescence emission intensity of 9-nitro-nos at this excitation wavelength was negligible. A 0.3-cm path-length cuvette was used to minimize the inner filter effects caused by the absorbance of 9-nitro-nos at higher concentration ranges. In addition, the inner filter effects were corrected using the formula $F_{corrected} = F_{observed} \cdot \text{antilog}[(A_{ex} + A_{em})/2]$, where A_{ex} is the absorbance at the excitation wavelength and A_{em} is the absorbance at the emission wavelength. The dissociation constant (K_d) was determined by the formula $1/B = K_d/[\text{free ligand}] + 1$, where B is the fractional occupancy and [free ligand] is the concentration of free noscapine or 9-nitro-nos. The fractional occupancy (B) was determined by the formula $B = \Delta F/\Delta F_{max}$, where ΔF is the change in fluorescence intensity when tubulin and its ligand are in equilibrium and ΔF_{max} is the value of maximum fluorescence change when tubulin is completely bound with its ligand. ΔF_{max} was calculated by plotting $1/\Delta F$ versus 1/ligand using total ligand concentration as the first estimate of free ligand concentration.

Tubulin Polymerization Assay

Mammalian brain tubulin (1.0 mg/ml) was mixed with different concentrations of 9-nitro-nos (25 or 100 μM) at 0°C in an assembly buffer (100 mM PIPES at pH 6.8, 3 mM $MgSO_4$, 1 mM EGTA, 1 mM GTP, and 1 M sodium glutamate). Polymerization was initiated by increasing the temperature to 37°C in a water bath. The rate and extent of the polymerization reaction were monitored by light scattering at 550 nm using a 0.3-cm path-length cuvette in a JASCO FP-6500 spectrofluorometer for 30 min.

In Vitro Cell Proliferation Assays

Sulforhodamine B Assay. The cell proliferation assay was performed in 96-well plates as described previously (Skehan et al., 1990; Zhou et al., 2003). Adherent cells (1A9 and 1A9/PTX22) were seeded in 96-well plates at a density of 5×10^3 cells/well. They were treated with increasing gradient concentrations of 9-nitro-nos the next day while in log-phase growth. After 72 h of drug treatment, cells were fixed with 50% trichloroacetic acid and stained with 0.4% sulforhodamine B dissolved in 1% acetic acid. Cells were then washed with 1% acetic acid to remove unbound dye. The protein-bound dye was extracted with 10 mM Tris base to determine the optical density at a 564-nm wavelength.

MTS Assay. Suspension cells (CEM, CEM/VLB100 and CEM/VM-1-5) were cultured in RPMI 1640 media containing 10% fetal bovine serum and then seeded into 96-well plates at a density of 5×10^3 cells/well and were treated with increasing gradient concentrations of 9-nitro-nos for 72 h. Measurement of cell proliferation was performed colorimetrically by 3-(4,5-dimethylthiazol-2-yl)-5-(3-carboxymethoxyphenyl)-2-(4-sulfophenyl)-2*H*-tetrazolium, inner salt (MTS) assay, using the CellTiter96 AQueous One Solution Reagent (Promega, Madison, WI). Cells were exposed to MTS for 3 h, and absorbance was measured using a microplate reader (Molecular Devices, Sunnyvale, CA) at an optical density of 490 nm. The percentage of cell survival as a function of drug concentration for both of the assays was then plotted to determine the IC_{50} value, which stands for the drug concentration needed to prevent cell proliferation by 50%.

Cell Cycle Analysis. The flow cytometric evaluation of the cell cycle status was performed as described previously (Zhou et al., 2003). In brief, 2×10^6 cells were centrifuged, washed twice with ice-cold phosphate-buffered saline (PBS), and fixed in 70% ethanol. Tubes containing the cell pellets were stored at 4°C for at least 24 h. Cells were then centrifuged at 1000*g* for 10 min, and the supernatant was discarded. The pellets were washed twice with 5 ml of PBS and then stained with 0.5 ml of propidium iodide (0.1% in 0.6% Triton-X in PBS) and 0.5 ml of RNase A (2 mg/ml) for 45 min in the dark. Samples were then analyzed on a FACSCalibur flow cytometer (Beckman Coulter Inc., Fullerton, CA).

Immunofluorescence Microscopy. Cells adhered to poly(L-lysine)-coated coverslips were treated with 9-nitro-nos for 72 h. After treatment, cells were fixed with cold (−20°C) methanol for 5 min and then washed with PBS for 5 min. Nonspecific sites were blocked by incubating with 100 μl of 2% BSA in PBS at 37°C for 15 min. A mouse monoclonal antibody against α-tubulin (DM1A; Sigma, St. Louis, MO) was diluted 1:500 in 2% BSA/PBS (100 μl) and incubated with the coverslips for 2 h at 37°C. Cells were then washed with 2% BSA/PBS for 10 min at room temperature before incubating with a 1:200 dilution of a fluorescein-isothiocyanate-labeled goat anti-mouse IgG antibody (Jackson ImmunoResearch, Inc., West Grove, PA) at 37°C for 1 h. Coverslips were then rinsed with 2% BSA/PBS for 10 min and incubated with propidium iodide (0.5 μg/ml) for 15 min at room temperature before they were mounted with Aqua-mount (Lerner Laboratories, Pittsburgh, PA) containing 0.01% 1,4-diazobicyclo(2,2,2)octane (Sigma). Cells were then examined using confocal microscopy for microtubule morphology and nuclear morphology to visualize DNA fragmentation (at least 100 cells were examined per condition).

Terminal Deoxynucleotidyl-Transferase-Mediated dUTP Nick-End Labeling Assay for Apoptosis. DNA strand breaks were identified by using the TUNEL assay as described previously (Bortner et al., 1995). In brief, 1A9/PTX22 cells were incubated with 50 μM 9-nitro-nos for 72 h. Cells were pelleted and washed with ice-cold PBS twice. Cells were then fixed in 1% paraformaldehyde, and apoptosis was detected using the APO-BrdU TUNEL Assay Kit from Invitrogen according to the manufacturer's instructions. In brief, cells were stained for a flow cytometry-based terminal deoxynucleotidyl transferase (TdT)-mediated bromo-deoxyuridine triphosphate (BrdUTP) reaction. The addition of BrdUTP to the TdT reaction provides a means to label the DNA strand breaks and is detected by an Alexa Fluor 488-labeled anti-BrdU antibody. DNA content was determined by the binding of DNA-specific dye, propidium iodide (x-axis). Apoptotic cells were determined by the incorporation of BrdU at the 3′-OH ends of the fragmented DNA as measured by anti-BrdU Alexa Fluor 488-labeled antibody on the y-axis. The number of apoptotic cells is indicated by the number of Alexa Fluor 488-positive cells of the total gated cells. This assay was run on a flow cytometer equipped with a 488-nm argon laser as the light

source. PI fluoresces at approximately 623 nm and Alexa-Fluor 488 at approximately 520 nm when excited at 488 nm. Single- and dual-parameter displays were created using the CellQuest Data Acquisition software (BD Biosciences, San Jose, CA). The gating display was the standard dual-parameter DNA doublet discrimination display, with the DNA area signal on the *y*-axis and the DNA width signal on the *x*-axis. From this display, a gate was generated around the nonclumped cells, and the second gated dual-parameter display was generated with the DNA (linear red fluorescence) on the *x*-axis and the Alexa-Fluor 488 (log green fluorescence) on the *y*-axis. Apoptotic cells were subsequently counted as those expressing high Alexa-Fluor 488 fluorescence. Confocal micrographs were also obtained for the TUNEL-stained cells using a 63× objective with a numerical aperture of 1.4.

Determination of Caspase-3 Activity. Cells (10^6) were incubated with 25 μM 9-nitro-nos (CEM, CEM/VLB100, and CEM/VM-1-5) or 50 μM 9-nitro-nos (1A9 and 1A9/PTX22) for 0, 24, 48, and 72 h. Caspase-3 activity was then measured by the cleavage of the small synthetic substrate *N*-benzyloxycarbonyl-Asp-Glu-Val-Asp-aminoluciferin (CaspaseGloTM 3/7 Assay System Kit; Promega) that becomes luminogenic upon cleavage. The luminescent signal, which is directly proportional to the amount of caspase-3 activity, was measured in a Luminoskan Ascent instrument after an incubation of 3 h (Thermo Electron).

Results

The nitration reaction is a well-studied electrophilic substitution reaction in organic chemistry. Although fuming nitric acid or 50% nitric acid in glacial acetic acid is extensively used for obtaining the nitrated product, the harsh oxidizing conditions of these reagents did not allow us to use these reagents for the nitration of noscapine. The lead compound, noscapine, comprises isoquinoline and benzofuranone ring systems joined by a labile C-C chiral bond, and both of these ring systems contain several vulnerable methoxy groups. Thus, achieving selective nitration at C-9 position without disruption and cleavage of these labile groups and C-C bonds was challenging. Treatment of noscapine with other nitrating agents like acetyl nitrate or benzoyl nitrate also resulted in epimerization or diastereoisomers (Lee, 2002). Next, we tried inorganic nitrate salts like ammonium nitrate or silver nitrate in the presence of acidic media to achieve aromatic nitration (Crivello, 1981). After carefully titrating several conditions and reagents, we successfully accomplished the nitration of noscapine using trifluoroacetic anhydride (TFAA). TFAA represents another commonly used reagent, and its extensive use is associated with its ability to generate a mixed anhydride, trifluoroacetyl nitrate, that is a reactive nitrating agent (Crivello, 1981). We also tried other reagents such as ammonium nitrate, sodium nitrate, or silver nitrate in chloroform, but those gave us low quantitative yields and had longer reaction times. Increased reaction rate and yields were obtained using a lower dielectric constant solvent, acetonitrile. The reaction was slightly exothermic and was completed in 1 h. The product remained in solution while the inorganic salt of trifluoroacetic acid precipitated and was removed by filtration.

Thus, 9-nitro-nos was prepared by the aromatic nitration of (*S*)-6,7-dimethoxy-3-((*R*)-4-methoxy-6-methyl-5,6,7,8-tetrahydro-[1,3]dioxolo[4,5-*g*]isoquinolin-5-yl)isobenzofuran-1(3*H*)-one (noscapine) using silver nitrate in acetonitrile and TFAA at 25°C (Fig. 1A). This method resulted in controlling the chemoselectivity of the reaction, in that aromatic substitution occurred at C-9 position of ring A of the isoquinoline nucleus. Absence of C-9 aromatic proton at δ 6.52 ppm in the ^{1}H NMR spectrum of the product confirmed the nitration at the C-9 position. Furthermore, ^{13}C NMR and HRMS data confirmed the structure of the compound.

9-Nitro-nos Binds Tubulin. Introduction of a nitro moiety in place of a proton usually disrupts the tight interactions within the ligand-binding pockets of proteins. Therefore, we first asked whether this novel compound, 9-nitro-nos, retains the tubulin binding activity of the parent compound, noscapine. Tubulin, like many other proteins, contains fluorescent amino acids like tryptophans and tyrosines. The intensity of the fluorescence emission is dependent on the microenviron-

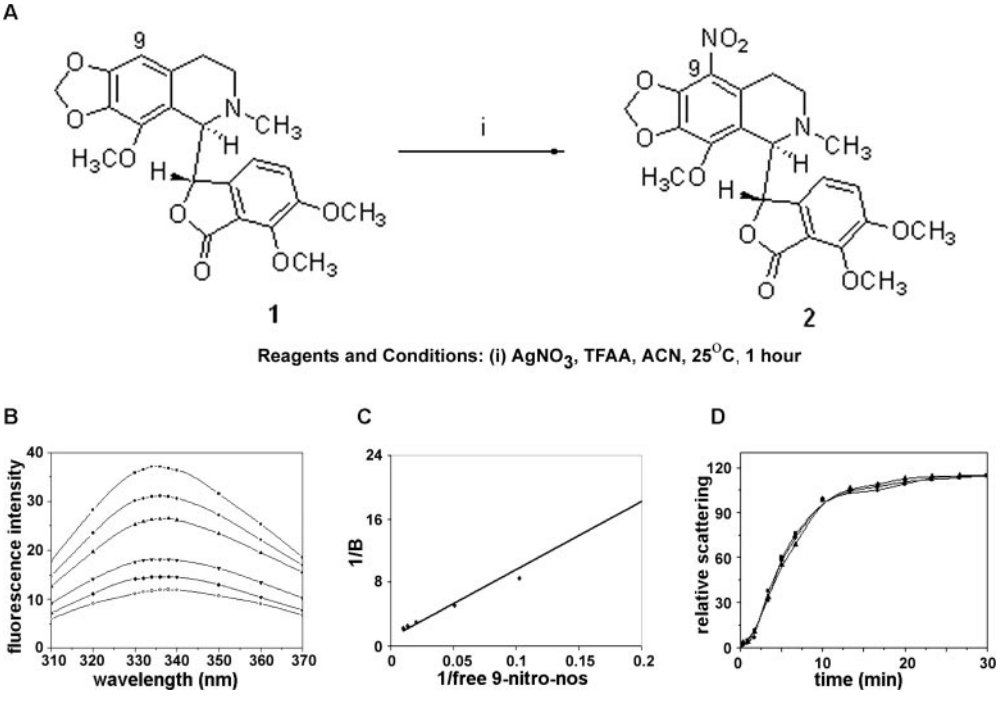

Fig. 1. A, synthesis of 9-nitro-noscapine. 9-Nitro-nos was synthesized by the aromatic nitration of noscapine using silver nitrate in acetonitrile and TFAA at 25°C. B, 9-nitro-nos binds tubulin. B shows the fluorescence-quenching spectrum of tubulin for 9-nitro-nos. ■, control; ●, 10 μM; ▲, 20 μM; ▼, 50 μM; ♦, 75 μM; and ○, 100 μM 9-nitro-nos. C, the double reciprocal plot which gives a K_d value of 86 ± 6 μM for 9-nitro-nos binding to tubulin. D, 9-nitro-nos does not significantly change the polymerization rate and the steady-state polymer mass of purified tubulin in vitro. The assay was based on the light-scattering ability of tubulin polymer, reflected as the absorbance at 550 nm wavelength. An equivalent amount of the solvent dimethyl sulfoxide was used as a negative control. ■, control; ●, 25 μM 9-nitro-nos; ▲, 100 μM 9-nitro-nos. Results are representative of four independent experiments.

ment around these amino acids in the folded protein. Agents that bind tubulin typically change the microenvironment and alter the fluorescent properties of the target protein (Peyrot et al., 1992; Panda et al., 1997; Ye et al., 1998). Measuring these fluorescent changes has become a standard method for determining the binding properties of tubulin ligands, including the classic compound colchicine (Peyrot et al., 1989; Andreu et al., 1991). We thus used this standard method to determine the dissociation constant (K_d) between tubulin and 9-nitro-nos compared with the carrier vehicle (dimethyl sulfoxide). Our results show that 9-nitro-nos quenched tubulin fluorescence in a saturable manner (Fig. 1B) and the double-reciprocal plot of these data revealed a K_d of 86 ± 6 μM for 9-nitro-nos binding to tubulin (Fig. 1C).

9-Nitro-nos Does Not Affect the Assembly Rate and Steady-State Monomer/Polymer Tubulin Mass. We next asked whether 9-nitro-nos promoted or inhibited microtubule polymerization. We have shown previously that noscapine does not significantly promote or inhibit microtubule polymerization upon binding tubulin, even at a concentration as high as 100 μM (Zhou et al., 2003). However, it does alter the steady-state dynamics of microtubule assembly, primarily by increasing the amount of time that the microtubules spend in an attenuated (pause) state (Zhou et al., 2002b). This property of noscapine makes it unique and has resulted in its extensive use to explore the role of microtubule dynamics during the spindle assembly checkpoint signaling. More importantly, it provides an advantage in that postmitotic cells, such as neurons, are not adversely affected by this drug even at higher concentrations. This is in contrast to the currently used anticancer drugs such as the family of taxanes and the vinca alkaloids, high micromolar concentrations of which cause devastating effects on cellular microtubules. We thus examined the effect of 9-nitro-nos on the assembly of tubulin subunits into microtubules in vitro by measuring the changes in the turbidity produced upon tubulin polymerization. Our results show that 9-nitro-nos did not inhibit the rate or extent of tubulin polymerization at 25 μM or even at concentrations as high as 100 μM (Fig. 1D). Having identified tubulin as the target molecule, we extended our pharmacology study at the cellular level to determine mechanisms by which 9-nitro-nos affects the cell cycle and induces cell death.

9-Nitro-nos Effectively Inhibits the Proliferation of Cancer Cells, Including Vinblastine-, Teniposide-, and Paclitaxel-Resistant Variants. Although many microtubule-binding drugs are active against many tumor types, most of these agents fail to manage the drug-resistant phenotypes of recurrent tumors. The NCI-60 cell panel shows a wide range of sensitivity for the parent compound noscapine; the drug-resistant variants, however, have not been explored fully. One major mechanism of acquired drug resistance is the overexpression of efflux pumps, namely Pgp170/MDR and MRP. For example, CEM/VLB100 cells, the Pgp-overexpressing vinblastine-resistant variants, show a 270-fold resistance to vinblastine (Beck and Cirtain, 1982) and CEM/VM-1-5 cells, the MRP-overexpressing variants, display a 400-fold resistance to teniposide (Morgan et al., 2000). We were surprised to note that 9-nitro-nos is active against the parental CEM cells and those of CEM-derived vinblastine- and teniposide-resistant cells, despite Pgp or MRP overexpression. We used an in vitro cell proliferation MTS assay to determine the drug concentration required to inhibit cell growth by 50% after incubation in the culture medium for 72 h. Our results show that the median inhibitory concentration (IC_{50}) of 9-nitro-nos for CEM, CEM/VLB100, and CEM/VM-1-5 cells is 10, 8.1, and 6.9 μM, respectively (Fig. 2). It is worth mentioning that the IC_{50} value for the drug-resistant sublines is lower than the parent line.

We next examined the effect of 9-nitro-nos on ovarian cancer cells, 1A9 and its paclitaxel-resistant variant 1A9/PTX22 (Giannakakou et al., 1997). Using a standard sulforhodamine B assay to evaluate the percentage of cell survival for these adherent cells, we found the IC_{50} value to be 30.1 and 27.5 μM for 1A9, the parent ovarian cancer cells, and 1A9/PTX22, the paclitaxel-resistant variant, respectively (Fig. 2). In the ovarian cancer cells also, we found that the IC_{50} value for the drug-resistant variant was lower than the parent cells. Like other microtubule-binding drugs, such as taxanes and epothilones, 9-nitro-nos is also quite effective against drug-resistant cells. Although the 1A9/PTX22 cells do not overexpress Pgp but rather have tubulin mutations that confer paclitaxel resistance, it is expected for 9-nitro-nos to display sensitivity toward drug-resistant cells because of a different binding pocket. 9-Nitro-nos has also been submitted by our laboratory for testing by the National Cancer Institute, through its Developmental Therapeutics Program, against their panel of 60 human cancer cell lines.

9-Nitro-nos Alters Cell Cycle Profile and Induces G_2/M Arrest in Cancer Cells. Microtubule-interfering agents, including noscapine (Ye et al., 1998; Zhou et al., 2002b), are well known to arrest cell cycle progression at the G_2/M phase in mammalian cells (Jordan and Wilson, 1999). Therefore, we next examined the effect of 9-nitro-nos on the percentage G_2/M and sub-G_1 cell populations of these cancer cells as a function of time. As can be seen in Fig. 3A, mitotic figures peak at approximately 24 to 48 h of drug exposure and then decrease after up to 72 h of observation. Consistent with this, the apoptotic cells increase in number during this time (Fig. 3B). Fluorescently labeled DNA accumulation is a good indicator of cell cycle progression and cell death. An

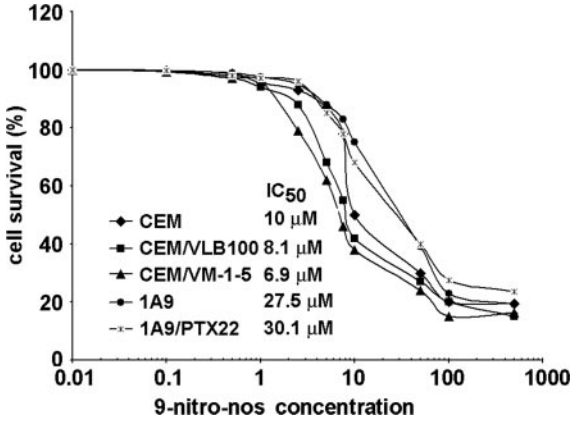

Fig. 2. 9-Nitro-nos actively inhibits the proliferation of various human cancer cells, including those that are resistant to vinblastine, teniposide, and paclitaxel. CEM, CEM/VLB100, CEM/VM-1-5, 1A9, and 1A9/PTX22 cells were treated with 9-nitro-nos at gradient concentrations for 72 h. The IC_{50} value was then measured using standard in vitro proliferation assays. The MTS assay was used for nonadherent suspension cells (CEM, CEM/VLB100, and CEM/VM-1-5), and the sulforhodamine B (SRB) assay was performed for adherent cells (1A9 and 1A9/PTX22). Each value represents the average of two independent experiments with five replicates each.

unreplicated complement of 2N DNA cells represents the G_1 phase, whereas duplicated 4N DNA cells represent G_2 and M phases. Cells in the process of DNA duplication between 2N and 4N peaks represent the S phase. Less than 2N DNA appears in populations of dying cells that degrade their DNA to different extents. Figure 3, C to G, depicts the flow cytometric profile of CEM, CEM/VLB100, CEM/VM-1-5, 1A9, and 1A9/PTX22 cells, respectively, treated with 9-nitro-nos for 0, 24, 48, and 72 h. Twenty-five micromolar 9-nitro-nos is used to study cell cycle profile in CEM, CEM/VLB1000, and CEM/VM-1-5 cells, whereas 50 μM 9-nitro-nos is used for 1A9 and 1A9/PTX22 cells. As is clearly evident from the three-dimensional fluorescence-activated cell sorting analysis (FACS) profiles, the display of DNA content as a function of time of drug exposure shows a pronounced increase in the population of cells that accumulate with less than 2N DNA (sub-G_1 population) at 72 h, indicating dying cells. This is preceded by an accumulation of cell populations with 4N DNA indicating G_2/M arrest. The anticancer activity of 9-nitro-nos treatment was thus evident in its ability to produce a significant sub-G_1 population, representing the fraction of cells which have hypodiploid (<2N) DNA content, typifying a cell population having degraded DNA, a characteristic of apoptosis. The effect of 9-nitro-nos on the progression of the entire cell cycle as a function of time shown as the percentage of G_0/G_1, S, G_2/M, and sub-G_1 populations in all three lymphoma cell lines and the two ovarian cell lines is shown in Table 1.

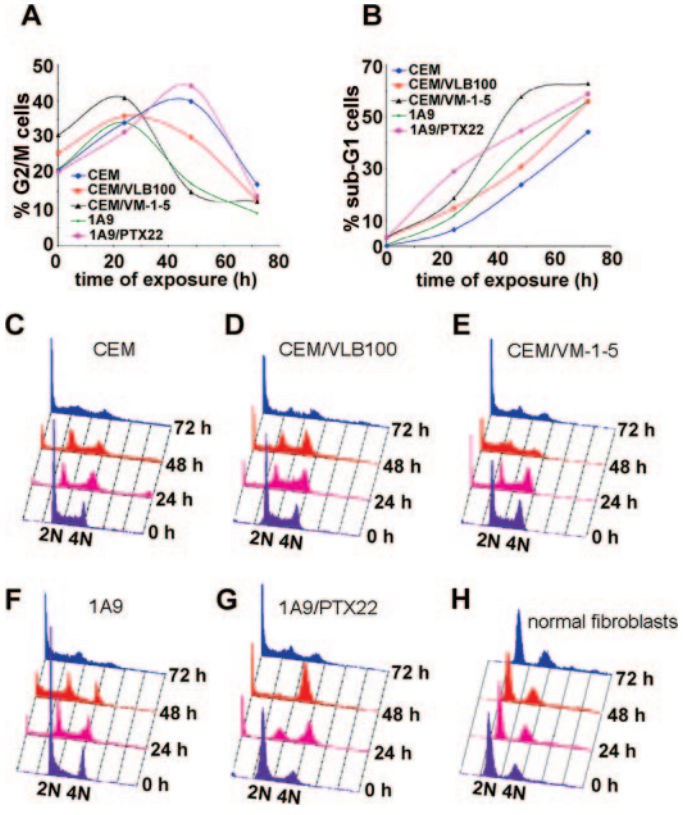

Fig. 3. 9-Nitro-nos arrests the cell cycle at G_2/M phase in human cancer cells. A and B, the percentage of G_2/M and sub-G_1 cells as a function of time of treatment with 9-nitro-nos. C to G show an increase in the population of cells with degraded DNA (sub-G_1 amount in the far left) in the three-dimensional FACS of DNA amounts. H, the effect of 9-nitro-nos on the cell cycle profile of normal primary fibroblast cells. Even concentrations as high as 100 μM did not alter the cell cycle progression profile of normal human cells. All cells were harvested for analysis at the indicated times, stained with propidium iodide, and analyzed by flow cytometry (FACS) using the CellQuest software. The *x*-axis shows intensity of PI fluorescence, which is indicative of the total DNA content of cells in different phases of the cell cycle. The *y*-axis represents the number of cells in each phase of the cell cycle, and the *z*-axis shows the time points 0, 24, 48, and 72 h. Results are representative of three experiments performed in triplicate.

Because the progression of normal cells through the cell cycle is tightly regulated by checkpoints, ensuring the exact replication of the genome during the S-phase and its precisely equal division at mitosis, we investigated whether 9-nitro-nos affects the cell cycle of the normal human fibroblast cells. We did not observe any perturbations in the cell cycle profile of normal fibroblast cells at even 100 μM 9-nitro-nos (Fig. 3H). It is surprising that 9-nitro-nos did not affect the cell cycle profile of human fibroblasts, whereas it did affect the cell cycle of primary melanocytes (Landen et al., 2002). Several possibilities exist. The first obvious possibility is that the primary fibroblasts are dormant and thus are not dividing. We do know, however, that these cells divide with a doubling time of approximately 18 to 20 h. The second very likely possibility comes from an astute observation by Rieder and colleagues (Mikhailov and Rieder, 2002), in which the authors make a clear case that cells in early stages of chromosome condensation (prometaphase) are reversible, in that drug-induced perturbations of microtubules can return cells from prometaphase to G_2 phase. The mechanism of this reversal is not well understood, and several laboratories, including ours, are investigating this intriguing observation. Thus, our in vitro studies with normal human cell cultures that show resistance to the apoptotic effects of 9-nitro-nos are in contrast to the adverse effects seen with human cancer cells.

Nevertheless, the cell cycle analyses suggest that the lymphoma and the ovarian cancer cells, including their drug-resistant variants, succumb to apoptosis upon treatment with 9-nitro-nos. Therefore, we went on to examine a variety of apoptotic events using several complementary cytometric and biochemical methods.

9-Nitro-nos Causes Extensive Apoptosis as Revealed by Immunocytochemistry. The onset of apoptosis characteristically changes cellular morphology. This includes membrane blebbing, formation of apoptotic bodies, disruption of cytoskeleton, and hypercondensation and fragmentation of chromatin. To visualize this, control untreated cells and cells treated with 9-nitro-nos for 72 h were analyzed by immunocytochemistry using a tubulin-specific antibody (green) and a DNA-binding dye (red). Confocal micrographs (Fig. 4A, top) shows control untreated CEM, CEM/VLB100, CEM/VM-1-5, 1A9, and 1A9/PTX22 cells. As expected, untreated control cells show normal radial microtubule arrays. In contrast, both lymphoma cells and ovarian cancer cells treated with 9-nitro-nos for 72 h show extensive terminal apoptotic figures with fragmented DNA pieces and perturbed microtubule arrays (Fig. 4A, bottom).

9-Nitro-nos Treatment Caused DNA Fragmentation as Measured Quantitatively by a Flow Cytometry-Based TUNEL Analysis. To further establish the apoptotic mechanism of cell death quantitatively, we next performed a flow cytometry based TUNEL assay in 1A9/PTX22 cells treated with 9-nitro-nos for 72 h. Because the end stages of apoptosis display cleaved 3′-ends of DNA, they can be visualized by specific labeling using TUNEL assay as an abun-

dant green staining (Fig. 4B, top right, open arrowheads; red denotes PI staining). The quantitative FACS analysis showed 55.9% TUNEL-positive cells within a population of 1A9/PTX22 cells treated with 50 μM 9-nitro-nos for 72 h (Fig. 4B, top left). In contrast, control untreated cells only occasionally show TUNEL-staining and TUNEL-negative cells appear red (Fig. 4B, bottom right, solid arrowhead). This is consistent with the quantitative FACS data that depict 95.9% control cells containing intact genomic DNA in the lower region of the cytogram representing the TUNEL-negative cells (Fig. 4B, bottom left). The other cell lines also showed similar results (data not shown). Although we do not know the precise mechanisms of the initial events that trigger apoptosis, we have shown the terminal stages by quantitating the 3′-ends of fragmented DNA as evidence of the execution phase of apoptosis.

9-Nitro-nos Causes Activation of Caspase-3, a Hallmark of Apoptosis, as a Function of Time. Caspases, the cysteine proteases, have been implicated as key participants in the sequence of events that result in the dismantling of the cell during apoptosis. The activation of caspase-3 is caused by upstream caspases and involves the cleavage of the inactive proenzyme into an active form. The active form can be monitored using a small peptide substrate which becomes luminogenic upon cleavage. As shown in Fig. 4C, we observed a concomitant time-dependent activation of caspase-3 as much as 10- to 20-fold in both the lymphoma cells and ovarian cancer cells, including their drug-resistant variants upon 72 h of 9-nitro-nos treatment. It is appreciated that the kinetics of caspase-3 activation depends very much on the nature of stimuli and the timing of misbalance in proapoptotic and antiapoptotic signals. As published earlier (Ye et al., 2001), it requires a long time of elevated p34cdc2 activity followed by the activation of c-Jun NH_2-terminal kinase pathway before caspase activation and apoptosis. Antimicrotubule drug induced caspase induction also somewhat depends on the generation time of cells. The cell lines we used had a doubling time ranging from approximately 20 to 48 h.

TABLE 1

Effect of 9-nitro-nos on cell cycle progression of drug-resistant cell lines and their normal counterparts

Cells were treated with 9-nitro-nos for the indicated times before being stained with propidium iodide for cell cycle analysis.

Cell Cycle Parameters	CEM				CEM/VLB100				CEM/VM-1-5				1A9				1A9/PTX22			
	0 h	24 h	48 h	72 h	0 h	24 h	48 h	72 h	0 h	24 h	48 h	72 h	0 h	24 h	48 h	72 h	0 h	24 h	48 h	72 h
	%																			
G_0/G_1	45.5	24.8	19.7	13.9	46.9	25.5	23.7	8.7	36.0	25.4	13.7	10.5	50.0	30.6	28.6	16.7	57.0	27.3	5.9	14.1
S	25.0	10.0	8.1	8.9	17.6	17.7	9.3	4.5	19.4	13.0	11.0	8.7	21.8	14.3	10.6	9.6	8.8	4.7	3.4	5.7
G_2/M	20.9	34.2	40.0	16.9	25.7	36.0	30.2	12.5	30.7	41.0	15.0	12.2	21.2	34.2	17.2	9.0	20.4	31.4	44.3	13.7
Sub-G_1	0.25	6.5	23.8	44.3	3.6	14.8	30.7	56.1	3.4	18.8	58.0	63.0	0.7	12.0	38.0	56.3	3.5	30.0	44.6	59.0

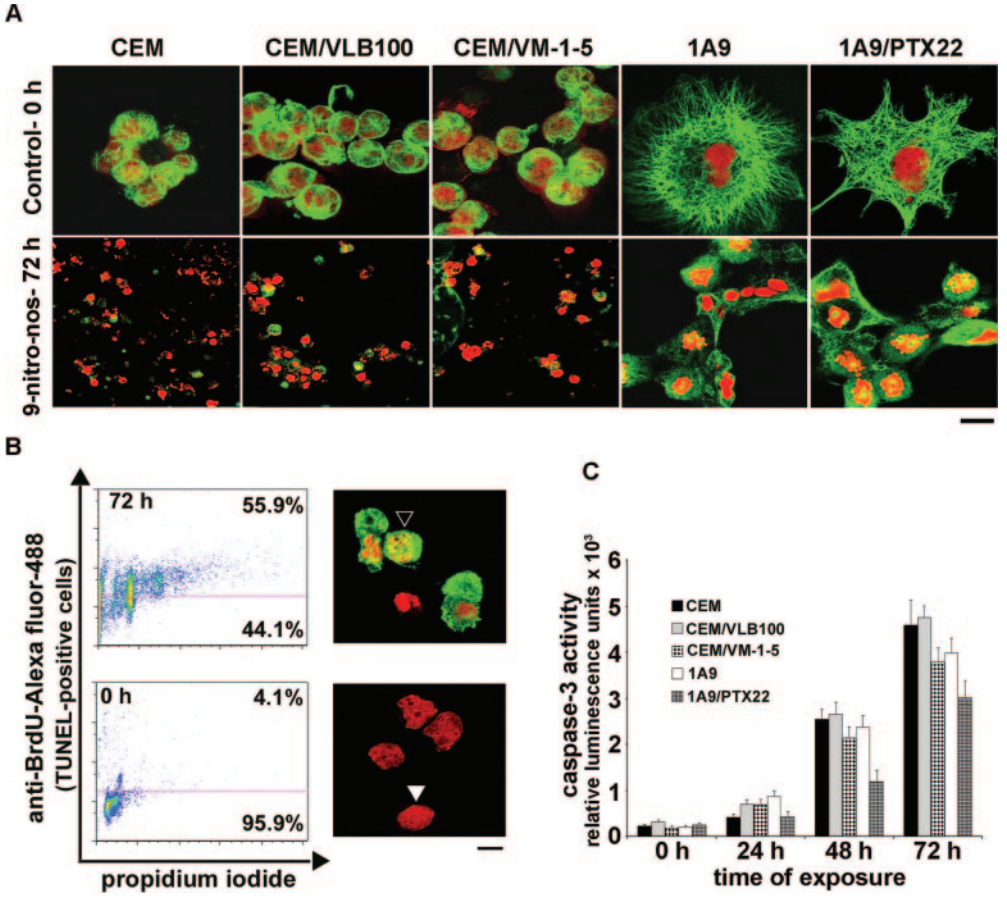

Fig. 4. 9-Nitro-nos kills cancer cells by inducing apoptosis. This is revealed by major changes in the nuclear morphology of these cells. A, top, untreated cells that display normal microtubule arrays. 9-Nitro-nos treatment for 72 h completely changes the morphologies, as seen by the fragmented condensed apoptotic bodies (A, bottom). Scale bar, 20 μM. B, the fragmented DNA in the terminal stages of apoptosis was measured using a flow cytometry-based quantitative TdT-mediated BrdUTP reaction (TUNEL assay) in a representative cell line (1A9/PTX22). Untreated control cells (bottom) and 50 μM 9-nitro-nos-treated 1A9/PTX22 cells (top) are shown. After 72 h of 9-nitro-nos treatment, cells were processed for apoptosis by a flow cytometry-based TUNEL assay. The fragmented DNA was also visualized using confocal microscopy as an abundance of TUNEL-positive cells (top right, open arrowhead). Untreated control cells appear red (bottom right, solid arrowhead). Scale bar, 20 μM. Data shown are from a representative experiment of two experiments performed. C, 9-nitro-nos treatment causes activation of caspase-3. The time-dependent increase in caspase-3 activity on 9-nitro-nos treatment in CEM, CEM/VLB100, CEM/VM-1-5, 1A9, and 1A9/PTX22 cells is shown. After drug incubation, caspase-3 activity was analyzed using the luminogenic substrate *N*-benzyloxycarbonyl-Asp-Glu-Val-Asp-aminoluciferin.

This is perfectly in line with our hypothesis that p34cdc2 activation in G_2/M block at approximately 24 h is sustained for approximately 20 h (perhaps because of a rather strong mitotic checkpoint) before the activation of stress-activated kinases such as c-Jun NH_2-terminal kinase. Although a direct and precise correlation between the generation time and caspase activation is difficult to derive, the timing of the appearance of TUNEL-stained cells can be directly correlated with the timing of caspase activation burst.

Discussion

Microtubule-interacting agents, both those that polymerize and bundle microtubules (such as *taxanes*) and depolymerize them, decreasing polymer mass (such as *vincas*), have been useful for the treatment of many cancer types. Unfortunately, the clinical success of these agents has been severely hampered by the emergence of drug resistance. Although patients show significant response to these drugs during treatment, most relapse and fail to respond to the same drug at a later stage. Multidrug resistance, by which cancer cells quite often become resistant to many structurally and mechanistically unrelated drugs, thus makes successful chemotherapy more complex and difficult to achieve (Gottesman, 2002). This phenomenon is primarily due to an enhanced efflux of drugs from the inside to the outside of cells by drug pumps, a family of ATP-binding cassette transporter proteins located on the cell membrane. P-glycoprotein, for example, is one such drug pump and is encoded by the multidrug resistance 1 gene. Overexpression of P-glycoprotein has been found to affect drug accumulation in the cell and correlates with the multidrug resistance phenotype in cancer cells (Gottesman and Pastan, 1993). Altered expression of tubulin isotypes is another contributing mechanism toward drug resistance (Burkhart et al., 2001) besides other unknown mechanisms. Another major challenge to successful chemotherapy by these antimicrotubule agents is associated toxicity. This is mainly because microtubules perform many other functions such as cytoplasmic organization and axonal transport, besides their function in chromosome movement during mitosis. Because the microtubule-targeting drugs currently in use either promote excessive stability of microtubules, such as the taxane family, or induce depolymerization of microtubules, like the vinca alkaloids, their usage is associated with various toxicities, such as gastrointestinal toxicity, alopecia, and peripheral neuropathy. A coupled aspect of the toxicity manifestation is their lack of specificity for dividing cells. Therefore, there has been a tremendous interest in identifying novel antimicrotubule agents that overcome various modes of resistance, display selectivity for cancer cells, and have safer pharmacology profiles.

Our laboratory discovered that noscapine is a unique antimicrotubule drug that alters microtubule dynamics without affecting the total polymer mass of tubulin and can be used successfully for probing the spindle assembly checkpoint mechanisms (Zhou et al., 2002b). In this study, we demonstrate that a nitro analog of noscapine, 9-nitro-nos, effectively inhibits cellular proliferation of lymphoma and ovarian cancer cells, in particular those that overexpress multidrug-resistant proteins. Furthermore, 9-nitro-nos significantly arrests cells at the G_2/M phase of the cell cycle followed by apoptotic cell death, as revealed by several prototypic features of apoptosis. Unlike currently used chemotherapeutics, 9-nitro-nos does not affect the cell cycle of normal human fibroblast cells. These findings thus indicate a great potential for the use of 9-nitro-nos as a chemotherapeutic agents for the treatment of human cancers, especially for those that are resistant to currently used microtubule drugs.

Acknowledgments

We thank Dr. William Beck for providing various CEM and its drug-resistant sublines used in this study and advice. We thank members of the Joshi laboratory for discussions. We are indebted to the anonymous reviewers of this manuscript for helpful suggestions.

References

Andreu JM, Gorbunoff MJ, Medrano FJ, Rossi M, and Timasheff SN (1991) Mechanism of colchicine binding to tubulin. Tolerance of substituents in ring C′ of biphenyl analogues. *Biochemistry* **30:**3777–3786.
Beck WT and Cirtain MC (1982) Continued expression of vinca alkaloid resistance by CCRF-CEM cells after treatment with tunicamycin or pronase. *Cancer Res* **42:**184–189.
Bortner CD, Oldenburg NBE, and Cidlowski JA (1995) The role of DNA fragmentation in apoptosis. *Trends Cell Biol* **5:**21–26.
Burkhart CA, Kavallaris M, and Horwitz SB (2001) The role of beta-tubulin isotypes in resistance to antimitotic drugs. *Biochim Biophys Acta* **1471:**1–9.
Checchi PM, Nettles JH, Zhou J, Snyder JP, and Joshi HC (2003) Microtubule-interacting drugs for cancer treatment. *Trends Pharmacol Sci* **24:**361–365.
Crivello JV (1981) Nitrations and oxidations with inorganic nitrate salts in trifluoroacetic anhydride. *J Org Chem* **46:**3056–3060.
Crown J and O'Leary M (2000) The taxanes: an update. *Lancet* **355:**1176–1178.
Dahlstrom B, Mellstrand T, Lofdahl CG, and Johansson M (1982) Pharmacokinetic properties of noscapine. *Eur J Clin Pharmacol* **22:**535–539.
Dumontet C, Isaac S, Souquet PJ, Bejui-Thivolet F, Pacheco Y, Peloux N, Frankfurter A, Luduena R, and Perol M (2005) Expression of class III beta tubulin in non-small cell lung cancer is correlated with resistance to taxane chemotherapy. *Bull Cancer* **92:**E25–E30.
Giannakakou P, Sackett DL, Kang YK, Zhan Z, Buters JT, Fojo T, and Poruchynsky MS (1997) Paclitaxel-resistant human ovarian cancer cells have mutant β-tubulins that exhibit impaired paclitaxel-driven polymerization. *J Biol Chem* **272:**17118–17125.
Gottesman MM (2002) Mechanisms of cancer drug resistance. *Annu Rev Med* **53:**615–627.
Gottesman MM and Pastan I (1993) Biochemistry of multidrug resistance mediated by the multidrug transporter. *Annu Rev Biochem* **62:**385–427.
Gupta K and Panda D (2002) Perturbation of microtubule polymerization by quercetin through tubulin binding: a novel mechanism of its antiproliferative activity. *Biochemistry* **41:**13029–13038.
Jensen LN, Christrup LL, Jacobsen L, Bonde J, and Bundgaard H (1992) Relative bioavailability in man of noscapine administered in lozenges and mixture. *Acta Pharm Nord* **4:**309–312.
Jordan MA and Wilson L (1999) The use and action of drugs in analyzing mitosis. *Methods Cell Biol* **61:**267–291.
Jordan MA and Wilson L (2004) Microtubules as a target for anticancer drugs. *Nat Rev Cancer* **4:**253–265.
Joshi HC (1998) Microtubule dynamics in living cells. *Curr Opin Cell Biol* **10:**35–44.
Joshi HC and Zhou J (2001) Gamma tubulin and microtubule nucleation in mammalian cells. *Methods Cell Biol* **67:**179–193.
Karlsson MO, Dahlstrom B, Eckernas SA, Johansson M, and Alm AT (1990) Pharmacokinetics of oral noscapine. *Eur J Clin Pharmacol* **39:**275–279.
Kirschner M and Mitchison TJ (1986) Beyond self-assembly: from microtubules to morphogenesis. *Cell* **45:**329–342.
Landen JW, Hau V, Wang MS, Davis T, Ciliax B, Wainer BH, Van Meir EG, Glass JD, Joshi HC, and Archer DR (2004) Noscapine crosses the blood-brain barrier and inhibits glioblastoma growth. *Clin Cancer Res* **10:**5187–5201.
Landen JW, Lang R, McMahon SJ, Rusan NM, Yvon AM, Adams AW, Sorcinelli MD, Campbell R, Bonaccorsi P, Ansel JC, et al. (2002) Noscapine alters microtubule dynamics in living cells and inhibits the progression of melanoma. *Cancer Res* **62:**4109–4114.
Lee D-U (2002) (−)-β-Narcotine: a facile synthesis and the degradation with ethyl chloroformate. *Bull Korean Chem Soc* **23:**1548–1552.
Mikhailov A and Rieder CL (2002) Cell cycle: stressed out of mitosis. *Curr Biol* **12:**R331–R333.
Monzo M, Rosell R, Sanchez JJ, Lee JS, O'Brate A, Gonzalez-Larriba JL, Alberola V, Lorenzo JC, Nunez L, Ro JY, et al. (1999) Paclitaxel resistance in non-small-cell lung cancer associated with beta-tubulin gene mutations. *J Clin Oncol* **17:**1786–1793.
Morgan SE, Kim R, Wang PC, Bhat U, Kusumoto H, Lu T, and Beck WT (2000) Differences in mutant p53 protein stability and functional activity in teniposide-sensitive and -resistant human leukemic CEM cells compared with parental CEM cells. *Oncogene* **19:**5010–5019.
Pace A, Bove L, Nistico C, Ranuzzi M, Innocenti P, Pietrangeli A, Terzoli E, and Jandolo B (1996) Vinorelbine neurotoxicity: clinical and neurophysiological findings in 23 patients. *J Neurol Neurosurg Psychiatry* **61:**409–411.
Panda D, Chakrabarti G, Hudson J, Pigg K, Miller HP, Wilson L, and Himes RH

(2000) Suppression of microtubule dynamic instability and tread milling by deuterium oxide. *Biochemistry* **39:**5075–5081.
Panda D, Singh JP, and Wilson L (1997) Suppression of microtubule dynamics by LY290181. *J Biol Chem* **272:**7681–7687.
Peyrot V, Leynadier D, Sarrazin M, Briand C, Menendez M, Laynez J, and Andreu JM (1992) Mechanism of binding of the new antimitotic drug MDL 27048 to the colchicine site of tubulin: equilibrium studies. *Biochemistry* **31:**11125–11132.
Peyrot V, Leynadier D, Sarrazin M, Briand C, Rodriquez A, Nieto JM, and Andreu JM (1989) Interaction of tubulin and cellular microtubules with the new antitumor drug MDL 27048. A powerful and reversible microtubule inhibitor. *J Biol Chem* **264:**21296–21301.
Ranganathan S, Dexter DW, Benetatos CA, Chapman AE, Tew KD, and Hudes GR (1996) Increase of beta(III)- and beta(IVa)-tubulin isotypes in human prostate carcinoma cells as a result of estramustine resistance. *Cancer Res* **56:**2584–2589.
Rowinsky EK (1997) The development and clinical utility of the taxane class of antimicrotubule chemotherapy agents. *Annu Rev Med* **48:**353–374.
Sammak PJ and Borisy GG (1987) Direct observation of microtubule dynamics in living cells. *Nature (Lond)* **332:**724–726.
Skehan P, Storeng R, Scudiero D, Monks A, McMahon J, Vistica D, Warren JT, Bokesch H, Kenney S, and Boyd MR (1990) New colorimetric cytotoxicity assay for anticancer-drug screening. *J Natl Cancer Inst* **82:**1107–1112.
Theiss C and Meller K (2000) Taxol impairs anterograde axonal transport of microinjected horseradish peroxidase in dorsal root ganglia neurons in vitro. *Cell Tissue Res* **299:**213–224.
Topp KS, Tanner KD, and Levine JD (2000) Damage to the cytoskeleton of large diameter sensory neurons and myelinated axons in vincristine-induced painful peripheral neuropathy in the rat. *J Comp Neurol* **424:**563–576.
Ye K, Ke Y, Keshava N, Shanks J, Kapp JA, Tekmal RR, Petros J, and Joshi HC (1998) Opium alkaloid noscapine is an antitumor agent that arrests metaphase and induces apoptosis in dividing cells. *Proc Natl Acad Sci USA* **95:**1601–1606.
Ye K, Zhou J, Landen JW, Bradbury EM, and Joshi HC (2001) Sustained activation of p34(cdc2) is required for noscapine-induced apoptosis. *J Biol Chem* **276:**46697–46700.
Zhou J and Giannakakou P (2005) Targeting microtubules for cancer chemotherapy. *Curr Med Chem Anticancer Agents* **5:**65–71.
Zhou J, Gupta K, Aggarwal S, Aneja R, Chandra R, Panda D, and Joshi HC (2003) Brominated derivatives of noscapine are potent microtubule-interfering agents that perturb mitosis and inhibit cell proliferation. *Mol Pharmacol* **63:**799–807.
Zhou J, Gupta K, Yao J, Ye K, Panda D, Giannakakou P, and Joshi HC (2002a) Paclitaxel-resistant human ovarian cancer cells undergo c-Jun NH_2-terminal kinase-mediated apoptosis in response to noscapine. *J Biol Chem* **277:**39777–39785.
Zhou J, Liu M, Aneja R, Chandra R, and Joshi HC (2004) Enhancement of paclitaxel-induced microtubule stabilization, mitotic arrest and apoptosis by the microtubule-targeting agent EM012. *Biochem Pharmacol* **68:**2435–2441.
Zhou J, Liu M, Luthra R, Jones J, Aneja R, Chandra R, Tekmal RR, and Joshi HC (2005) EM012, a microtubule-interfering agent, inhibits the progression of multidrug-resistant human ovarian cancer both in cultured cells and in athymic nude mice. *Cancer Chemother Pharmacol* **55:**461–465.
Zhou J, Panda D, Landen JW, Wilson L, and Joshi HC (2002b) Minor alteration of microtubule dynamics causes loss of tension across kinetochore pairs and activates the spindle checkpoint. *J Biol Chem* **277:**17200–17208.

Address correspondence to: Dr. Harish C. Joshi, Department of Cell Biology, Emory University School of Medicine, Laboratory for Drug Discovery and Research, 615 Michael St., Atlanta, GA 30322. E-mail: joshi@cellbio.emory.edu